Astron. Astrophys. 327, 377–387 (1997)

ASTRONOMY
AND
ASTROPHYSICS

Magnetoacoustic wave propagation in current sheets

J.M. Smith[1], **B. Roberts**[1], **and R. Oliver**[2]

[1] School of Mathematical and Computational Sciences, University of St Andrews, North Haugh, St Andrews, Fife KY16 9SS, UK
[2] Departament de Física, Universitat de les Illes Balears, E-07071 Palma de Mallorca, Spain

Received 13 February 1997 / Accepted 28 March 1997

Abstract. Magnetoacoustic waves in a Harris neutral current sheet are investigated. The magnetic field strength, Alfvén speed, sound speed and plasma density vary continuously across the structure. The sheet supports body, surface and hybrid modes. Two surface modes exist (a kink and a sausage). In addition, fundamental and harmonic body waves are found when their phase speeds approach the maximum Alfvén speed in the sheet. As the phase speeds of the modes decrease, the waves have properties of both body and surface modes – a hybrid wave. In the long wavelength limit the phase speed of the fundamental kink body mode and sausage surface mode approach the maximum Alfvén and tube speeds respectively. At short wavelengths, the phase speeds tend to constant values, each pair of kink and sausage modes merging after passing through the maximum value of the sound speed, c_s^{max}. For all modes, in the inner part of the current sheet, the gas pressure is out of phase with the magnetic pressure, with the gas pressure dominating (a property of a slow mode). In the outer part of the sheet the magnetic pressure is in phase with the total pressure (a fast mode characteristic). No purely fast or slow mode exists. For uniform density a minimum in the group velocity occurs only for the fundamental kink mode. For the Epstein density profile, minima in the group velocity are found for the other modes also. Impulsively generated waves are expected to show temporal variations that are similar to observations of oscillations of radio and X-ray emission of the solar corona and neutral sheet oscillations in the Earth's magnetotail. Calculated periods of oscillation are in good agreement with observations.

Key words: MHD – Sun: corona – Sun: magnetic field – Sun: oscillations – solar system: Earth

1. Introduction

Neutral sheets may guide waves. Ducted waves occur in regions of low Alfvén speed (see Edwin & Roberts 1982; Roberts, Edwin & Benz 1984; Murawski & Roberts 1993a,b; Nakariakov & Roberts 1995; Smith, Roberts & Oliver 1997). Therefore we may expect wave energy to be localised where the magnetic field is weak, as in a neutral sheet, or where plasma density is high, as within a coronal loop. Hence coronal streamers, which contain both closed dense loops and current sheets, are expected to provide effective wave ducts. The investigation of magnetoacoustic wave propagation in inhomogeneous photospheric flux tubes and coronal loops has been comprehensively studied (see the reviews by Roberts 1985, 1991, 1992 and Edwin 1991, 1992). A variety of waves may be present in the solar atmosphere – body or surface, fast or slow – their existence and properties depending upon the relative orderings of the Alfvén and sound speeds.

Direct observations of current sheets in the solar atmosphere are not common. Eddy (1973), analysing results from the 1922 eclipse, suggests the existence of a coronal neutral sheet which separates regions of opposite magnetic polarity. The width and length of the sheet were found to be 9 arc-seconds and 4 solar radii respectively. Neutral sheets are expected to be present above the helmet structures in coronal streamers and between coronal loop systems of opposite polarity. Current sheets may be formed in one of three ways (Priest 1982): the interaction of topologically distinct regions, the loss of equilibrium of a force-free field, and X-point collapse. In addition, in the Earth's magnetosphere, the nightside central plasma sheet and dayside magnetopause both contain current sheets. We show here that such sheets may support magnetoacoustic waves.

Current sheets are important structures which may guide waves; the damping of these waves may be an important mechanism for coronal heating (see, for example, Cramer 1994; Tirry, Čadež & Goossens 1997). The study of magnetoacoustic waves in current sheets may also provide valuable insight into the origin of certain frequently reported oscillations in the corona (Aschwanden 1987; Tsubaki 1988) and the Earth's magnetosphere (see Anderson 1994 and references therein). Evidence of wave-like motions in solar current sheets is limited, although Aurass & Kliem (1992) associate a Type IV radio burst with activity in a large sheet. These authors suggest that the formation of current filaments by the tearing mode instability may create propagating magnetoacoustic waves. In addition, there have been many recent observations of short period coronal oscillations (Correia & Kaufmann 1987; Zhao et al. 1990; Rušin & Minarovjech 1994;

Send offprint requests to: J.M. Smith

Zlobec et al. 1992), with periods ranging from 0.3 to 12 seconds, which may be associated with oscillating current sheets. There have also been reports of current sheet oscillations in the Earth's magnetotail. Periodicities in the range 3.5 to 5 minutes in the electron flux were reported by Montgomery (1968). Mihalov, Sonett & Colburn (1970) found periods ranging from 0.5 to 15 minutes with peaks at 100 seconds, 4.5 minutes and 8 minutes. Recently, Bauer, Baumjohann & Treumann (1995a) and Bauer et al. (1995b) have reported 1-2 minute oscillations in the vicinity of the current sheet where the perturbed gas and magnetic pressures were out of phase.

Several authors have investigated wave propagation in neutral sheets (see the review article by Cramer 1995). Hopcraft & Smith (1985) solved the governing wave equation for a Harris sheet analytically through a small parameter expansion. Although dispersion curves for fast magnetoacoustic waves were presented, the validity of the expansion near the edge of the sheet is uncertain. Further work by Hopcraft & Smith (1986) solved the governing wave equation numerically, although no dispersion curves were given. The magnetic field and pressure profiles used by Hopcraft & Smith (1986) were discontinuous at the sheet boundary. Although the sheet was in equilibrium an additional current at the edge of the sheet was generated which may have affected the results. Using the Harris sheet model, Seboldt (1990) investigated the singular solutions of the governing wave equation. This analysis showed that perturbations may be subject to phase mixing. Discrete eigenmodes were also briefly discussed, although no detailed analysis of the modes was given. Cramer (1994) examined the Alfvén and slow resonances of surface waves in a current sheet. The sheet was modelled as a field with an arbitrary change of direction through a narrow transition region. Cramer found that for certain angles of propagation surface waves were non-existent; two surface waves were present for some angles of propagation (compare with Roberts 1981a). The recent investigation by Tirry, Čadež & Goossens (1997) explored the damping of surface waves in a Harris profile through the Alfvén resonance; they found only two surface modes existed (the kink and sausage), with the sausage mode undergoing more damping than the kink.

A simple model of a current sheet was analysed by Edwin, Roberts & Hughes (1986) and Edwin (1992) to explain the generation of Pi2 pulsations in the plasma sheet. These oscillations are quasi-periodic pulsations with periods ranging between 40 and 150 seconds, typically lasting for a few cycles (Southwood & Stuart 1980; Singer et al. 1985). The sheet was modelled as an unbounded hot plasma slab, with a narrow field-free region, between the anti-parallel fields of the magnetotail. In the magnetic region the cold plasma approximation was used. Both fundamental kink body and sausage surface modes were found. In the slender sheet approximation, their phase speeds tended towards the exterior Alfvén and tube speeds, respectively. The fundamental kink body mode transforms to a surface wave when its phase speed falls below the constant sound speed within the sheet. Taking the velocity component v_x normal to the equilibrium magnetic field and the total pressure perturbation both continuous across the sheet boundary at $x{=}\pm a$ leads to the dispersion relations (assuming $v_x \to 0$ as $|x| \to \infty$) (Edwin et al. 1986; Edwin 1992)

$$\frac{2}{\gamma R^2}\left(k_z^2 v_{Ae}^2 - \omega^2\right) m_o \left\{ \begin{array}{c} \tanh \\ \coth \end{array} \right\} m_o a = \omega^2 m_e \tag{1}$$

for the surface $\left(m_o^2 > 0\right)$ modes, and

$$\frac{2}{\gamma R^2}\left(k_z^2 v_{Ae}^2 - \omega^2\right) n_o \left\{ \begin{array}{c} -\tan \\ \cot \end{array} \right\} n_o a = \omega^2 m_e \tag{2}$$

for the body $\left(n_o^2 = -m_o^2 > 0\right)$ waves. Here

$$m_i^2 = -n_i^2 = \frac{\left(k_z^2 c_{si}^2 - \omega^2\right)\left(k_z^2 v_{Ai}^2 - \omega^2\right)}{k_z^2 c_{si}^2 v_{Ai}^2 - \left(c_{si}^2 + v_{Ai}^2\right)\omega^2} \; ; \tag{3}$$

the subscript i equals o in the field-free region and e in the magnetic region. The 'tan' and 'tanh' solutions refer to the sausage mode, whereas the 'cot' and 'coth' terms relate to kink modes. The frequency and longitudinal wavenumber are ω and k_z, respectively, whilst the sound and Alfvén speeds are denoted by c_{si} and v_{Ai}. γ is the ratio of specific heats and R is the ratio of exterior Alfvén speed to interior sound speed. The dispersion diagram is discussed later (see Fig. 3b).

The dimensionless phase speed of both sausage and kink surface waves, $v_{ph} = \omega / k_z v_{Ae}$, tends to the same limiting value at short wavelengths ($k_z a \gg 1, \tanh m_o a, \coth m_o a \to 1$), given by (Edwin et al. 1986)

$$v_{ph}^4 \left[\left(\frac{R^2 \gamma}{2} \right)^2 - R^2 \right] + v_{ph}^2 \left(R^2 + 1 \right) - 1 = 0 \; , \; R = \frac{v_{Ae}}{c_{so}} \; . \tag{4}$$

(There is a spurious solution to Eq. (4) which does not satisfy the original dispersion relation.) In addition, sausage and kink body modes were found above wavenumber cut-offs. The phase speed of these body waves lie between the interior sound speed c_{so} and the exterior Alfvén speed v_{Ae}. Edwin et al. (1986) and Edwin (1992) suggested the long period magnetospheric oscillations (see, for example, Anderson 1994) may be due to surface waves, whereas the shorter period Pi2 pulsations may be body waves (see also McKenzie 1970 for a similar model). Impulsively generated waves in a plasma sheet were found to consist of a well defined wave packet consisting of a periodic phase, followed by quasi-periodic phase and then a decay phase, in good agreement with observations. However, an important aspect neglected in this model was the field reversal region. It is the purpose of this paper to consider propagation in a structured current sheet.

In this paper we investigate in detail the eigenmodes supported by a current sheet. Such an investigation may provide important seismic information about the corona and magnetosphere. We show that a current sheet supports both kink and sausage oscillations. In the sausage mode the current sheet pulsates like a blood vessel, with the central axis remaining undisturbed. In the kink mode the central axis moves back and forth during the wave motion. In a simple slab, modes may also be characterised as either *body* (oscillatory in the

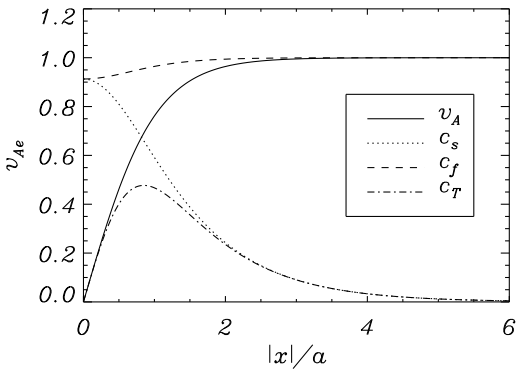

Fig. 1. A plot of the Alfvén v_A, sound c_s, fast c_f and tube c_T speeds (normalised against v_{Ae}) in a neutral current sheet with uniform density and γ=5/3. The region of low Alfvén speed about $x/a = 0$ acts as a duct for magnetoacoustic waves. Note that the fast speed is approximately constant throughout the whole domain. The sound and tube speeds have maxima of $0.9129 v_{Ae}$ and $0.4771 v_{Ae}$, respectively. These speeds are important in determining the nature of the magnetoacoustic waves in a current sheet.

interior) or *surface* (hyperbolic in the interior); see Roberts (1981a,b,1985,1991,1992), Edwin & Roberts (1982) and Edwin (1991, 1992) for a full discussion. We show that in a continuously structured medium, three types of mode can exist: *body*, *surface* and *hybrid*. The nature of the mode is governed by the phase speed and wavenumber. Hybrid modes contain elements of both body and surface waves. We restrict attention to modes which are evanescent outside the current sheet and therefore ignore any wave leakage (see, for example, Cally 1986).

The component of velocity transverse to the sheet can have nodes in two spatial directions, across the sheet width or along the sheet length. Modes with the least number of nodes across the sheet are referred to as fundamental modes. Traversing the sheet from one boundary to the other, the velocity in the fundamental kink mode does not change sign whereas the fundamental sausage mode changes sign once (at the central axis). Overtones of the kink and sausage modes have a greater number of nodes in the direction perpendicular to the current sheet axis.

For the neutral sheet in the Earth's magnetotail, widths of 3-6 R_E ($R_E \approx 6400$ km) have been used by Patel (1968), McKenzie (1970) and Edwin et al. (1986) in theoretical models. Hopcraft & Smith (1985) used a range from 1000 km to 50,000 km, whilst Seboldt (1990) used a sheet thickness of 30,000 km. For our calculations we use current sheet widths of $2a$ = 1000 km for solar applications and $2a = R_E$ for the Earth's magnetotail. The constant Alfvén speed in the corona is taken to be 1000 km s^{-1}, whilst in the magnetosphere a value of 500 km s^{-1} is considered (Mihalov et al. 1970). In this paper we use the standard ideal magnetohydrodynamic (MHD) equations. The mean free path in the solar corona (for temperatures 10^6 K and number densities 10^9 cm^{-3}) is of the order of 50 km whereas the electron gyro-radius is 20 cm for a field of 1G (Spitzer 1962). Hence, we consider only current sheets with widths greatly in excess of 50 km to ensure the validity of MHD. Ideal MHD may only be applied with caution in the Earth's magnetosphere. A discussion on the validity of the use of MHD in the magnetosphere may be found in Schindler and Birn (1978, 1986) and Birn, Hesse and Schindler (1996). The authors suggest that a MHD approach may be justified because the plasma pressure is approximately isotropic within the plasma sheet. In addition, Birn et al. (1996) compare the results of simulations of the magnetotail using MHD, hybrid and particle codes. The results are qualitively similar in each case, suggesting MHD is a good approximation to the more rigourous particle treatment.

The format of the paper is as follows. In Sect. 2 the equilibrium and governing wave equation are discussed. In Sect. 3 the numerical procedure for solving the wave equation is described. In Sect. 4 we explain the properties of magnetoacoustic waves in current sheets and in Sect. 5 our conclusions and applications are made.

2. Equilibrium and governing equations

Consider a current sheet in equilibrium modelled using a Harris profile (Harris 1962). The one-dimensional magnetic field is given by

$$\mathbf{B} = B_e \tanh\left(\frac{x}{a}\right) \hat{\mathbf{e}}_\mathbf{z} \ , \tag{5}$$

representing a continuous change of the magnitude of the field from B_e at large positive x/a to $-B_e$ at large negative x/a and passing through zero at x/a=0. Equilibrium demands that the total pressure (plasma plus magnetic) is uniform:

$$p(x) + \frac{B^2(x)}{2\mu} = constant \ , \tag{6}$$

yielding a plasma pressure $p(x)$ given by

$$p(x) = p_o \mathrm{sech}^2\left(\frac{x}{a}\right) \ , \qquad p_o = B_e^2/2\mu \ , \tag{7}$$

given that $p \to 0$ (cold plasma) as $|x|/a \to \infty$. The plasma density is arbitrary; we assume a density profile $\rho(x)$ of the form (cf. Epstein 1930)

$$\rho(x) = \rho_o \mathrm{sech}^2\left(\frac{x}{a}\right) + \rho_e \tanh^2\left(\frac{x}{a}\right) \ , \tag{8}$$

declining from ρ_o at $x/a = 0$ to $\rho_e\,(< \rho_o)$ as $|x|/a \to \infty$. Through the ideal gas law ($p \propto \rho T$), the temperature $T(x)$ is non-isothermal. The implied sound speed $c_s(x)$ $\left(= \left(\gamma p/\rho\right)^{1/2}\right)$ varies from $c_s(0)$ at the centre of the current sheet to zero in the far environment of the sheet, consistent with our assumption of a cold plasma as $|x| \to \infty$. Specifically, the square of the sound speed $c_s^2(x)$ is given by

$$c_s^2(x) = \frac{c_s^2(0)\,\mathrm{sech}^2\left(\frac{x}{a}\right)}{\frac{\rho_o}{\rho_e}\mathrm{sech}^2\left(\frac{x}{a}\right) + \tanh^2\left(\frac{x}{a}\right)} \ . \tag{9}$$

The square of the Alfvén speed $v_A^2(x)$ $\left(= B^2/\mu_o\rho\right)$ is given by

$$v_A^2(x) = \frac{v_{Ae}^2 \tanh^2\left(\frac{x}{a}\right)}{\frac{\rho_o}{\rho_e}\mathrm{sech}^2\left(\frac{x}{a}\right) + \tanh^2\left(\frac{x}{a}\right)} \ , \tag{10}$$

where $v_{Ae}^2 = {B_e}^2/\mu\rho_e = 2c_s^2(0)/\gamma$. Thus the Alfvén speed $v_A(x)$ declines from v_{Ae} in the far environment of the current sheet $\left(|x|/a \to \infty\right)$ to zero at the centre of the sheet. Fig. 1 gives plots of these two speeds, together with the tube speed $c_T(x)$ $\left(= c_s v_A/(c_s^2 + v_A^2)^{1/2}\right)$ and the fast speed $c_f(x)$ $\left(= (c_s^2 + v_A^2)^{1/2}\right)$, using $\gamma = 5/3$. The equilibrium condition (6) may be written in the alternative form

$$\rho(x)\left[\frac{2}{\gamma}c_s^2(x) + v_A^2(x)\right] = constant\ . \tag{11}$$

The Alfvén and sound speed profiles alongwith the density profile satisfies the equilibrium condition (11).

Consider the linearised equations of ideal magnetohydrodynamics, assuming gravity is negligible. The wave equation for plasma motions,

$$\mathbf{v} = (v_x, 0, v_z)\exp i(\omega t - k_z z)\ , \tag{12}$$

in a non-uniform magnetic field $\mathbf{B} = B(x)\,\hat{\mathbf{e}}_\mathbf{z}$ where the equilibrium parameters (density and pressure) are dependent upon x is given by (Roberts 1981a)

$$\frac{\mathrm{d}}{\mathrm{d}x}\left[f(x)\frac{\mathrm{d}v_x}{\mathrm{d}x}\right] + \rho\left(\omega^2 - k_z^2 v_A^2\right)v_x = 0\ , \tag{13}$$

where

$$f = \frac{\rho c_f^2\left(\omega^2 - k_z^2 c_T^2\right)}{\left(\omega^2 - k_z^2 c_s^2\right)}\ . \tag{14}$$

Here v_x is the velocity component normal to the magnetic field, ω is the frequency and k_z is the longitudinal wavenumber along the sheet. The velocity parallel to the magnetic field is given by

$$v_z = -\frac{ik_z c_s^2}{\left(\omega^2 - k_z^2 c_s^2\right)}\frac{\mathrm{d}v_x}{\mathrm{d}x}\ . \tag{15}$$

We consider only motions that are independent of the y-coordinate so that propagation is in the xz-plane.

The perturbed gas (p_1), magnetic $\left(p_{1m} = \mathbf{B}\cdot\mathbf{b_1}/\mu\right)$ and total p_T (gas and magnetic) pressure perturbations are given by

$$\frac{i\omega}{\rho}p_1 = -\frac{c_s^2\omega^2}{\left(\omega^2 - k_z^2 c_s^2\right)}\frac{\mathrm{d}v_x}{\mathrm{d}x} - \frac{v_x}{\rho}\frac{\mathrm{d}p}{\mathrm{d}x}\ , \tag{16}$$

$$\frac{i\omega}{\rho}p_{1m} = -v_A^2\frac{\mathrm{d}v_x}{\mathrm{d}x} - \frac{B}{\mu\rho}\left(\frac{\mathrm{d}B}{\mathrm{d}x}\right)v_x\ , \tag{17}$$

$$\frac{i\omega}{\rho}p_T = -\frac{c_f^2\left(\omega^2 - k_z^2 c_T^2\right)}{\left(\omega^2 - k_z^2 c_s^2\right)}\frac{\mathrm{d}v_x}{\mathrm{d}x}\ , \tag{18}$$

whilst the magnetic tension force $\mathbf{T_1}$ takes the form

$$\frac{i\omega}{\rho}\mathbf{T_1} = -v_A^2 k_z^2 v_x\hat{\mathbf{e}}_\mathbf{x} + \left(\omega^2 - k_z^2 c_s^2\right)\frac{v_A^2}{c_s^2}v_z\hat{\mathbf{e}}_\mathbf{z}\ , \tag{19}$$

where $\mathbf{b_1}$ is the perturbed magnetic field and

$$\mathbf{T_1} = \frac{1}{\mu}(\mathbf{B}\cdot\nabla)\,\mathbf{b_1} + \frac{1}{\mu}(\mathbf{b_1}\cdot\nabla)\,\mathbf{B}\ . \tag{20}$$

To investigate the nature of the modes we reduce Eq. (13) to the canonical form. Setting $v_x = \phi(x)\,F(x)$ reduces the governing wave equation to

$$\phi'' + \kappa^2(x)\,\phi = 0\ ,\ \kappa^2 = -m_i^2 - \frac{1}{2}\left(\frac{f'}{f}\right)' - \frac{1}{4}\left(\frac{f'}{f}\right)^2\ , \tag{21}$$

with m_i^2 given by Eq. (3) and $F'/F = \left(-1/2\right)f'/f$, with f given by Eq. (14). Here the dash denotes a derivative with respect to x. For a uniform medium, κ^2 is constant $\left(= -m_i^2\right)$; body and surface modes are determined by positive and negative κ^2, respectively. However, for a medium which is continuously structured, we define *body* and *surface* modes when κ^2 attains positive or negative values, respectively, across the whole sheet $(-a < x < a)$. In addition, *hybrid* modes occur when $\phi(x)$ possesses both positive and negative κ^2 across the width of the sheet.

3. Numerical procedure and boundary conditions

We solve Eq. (13) numerically subject to boundary conditions at the centre of the sheet, so that one has control over the parity of the solution (kink or sausage). At $x = x_{max}$ we take v_x to be zero; the integration range is therefore $[0, x_{max}]$. Lengths and speeds are normalised against the half-width a of the sheet and the Alfvén speed v_{Ae} in the exterior; frequencies are measured in units of v_{Ae}/a. The second order ordinary differential equation (13) is written in terms of two first order equations in the new functions y_1 and y_2:

$$y_1 = f(x)\frac{\mathrm{d}v_x}{\mathrm{d}x}\ ,\qquad y_2 = v_x\ , \tag{22}$$

such that

$$\frac{\mathrm{d}y_1}{\mathrm{d}x} = \rho\left(k_z^2 v_A^2 - \omega^2\right)y_2\ ,\qquad \frac{\mathrm{d}y_2}{\mathrm{d}x} = \frac{y_1}{f(x)}\ . \tag{23}$$

The boundary conditions at $x/a = 0$ for the kink mode are given by $y_1 = 0$, $y_2 = c$; for the sausage mode, $y_1 = cf(0)$ and $y_2 = 0$ at $x/a = 0$. The constant c is arbitrary. We impose that v_x is zero at $x = x_{max}$ for both modes.

To obtain a solution of the Eq. (13) we use a fixed value of k_z and integrate the two first order equations (22) using the NAG routine D02BEF. The integration is performed between $x = 0$, where proper initial conditions for y_1 and y_2 are available, and x_{max}, where the condition $v_x = 0$ must be satisfied. A Newton iteration, with NAG routine C05AXF, is done by changing $\omega a/v_{Ae}$ and integrating from $x = 0$ to $x = x_{max}$ until the boundary condition at the second point is satisfied. The value of x_{max} is chosen to be large, typically $x_{max} = 100a$, except for short wavelengths where it was found that a smaller x_{max} (e.g. $10a$) worked better. For long (short) wavelengths the integration range is wide (narrow), in such a way that the frequencies and eigenfunctions are not affected by the boundaries. On locating a solution to Eq. (13), the velocity is examined in the exterior of the sheet. We consider only those solutions where the velocity decreases to zero outside the sheet, thus imposing an exponentially decreasing solution. We have made a

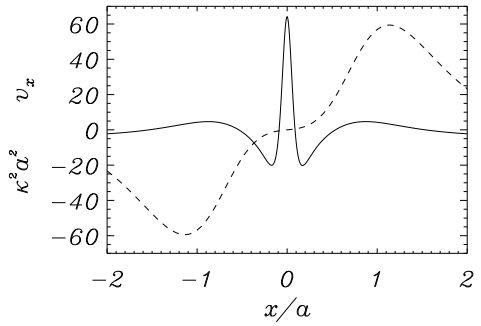

Fig. 2. The variation of the function $a^2\kappa^2(x)$ across the current sheet for a fundamental sausage hybrid mode with wavenumber $k_z a$ = 5.0 and phase speed ω/k_z=0.92 v_{Ae} (solid line). The corresponding x-component of velocity (dashed line) is scaled so the maximum velocity is 60. Note that regions of both positive (body type) and negative (surface type) $\kappa^2 a^2$ exist; the mode is hybrid.

careful comparison (see Smith 1997) of the results produced by this numerical procedure and those obtained analytically for the simpler problem of a magnetic slab (discussed by Edwin et al. 1986) and found excellent agreement, so we are confident that the procedure correctly determines the evanescent modes of a current sheet.

4. Results

4.1. Uniform density

We begin by looking at the various modes which may propagate in a current sheet. The function κ^2 arising in Eq. (21) is strongly dependent upon the mode of oscillation (wavenumber and phase speed) and also the position along the sheet. We find that three types of mode may exist in a continuously structured sheet, compared with two in a simple slab. Modes of oscillation may have $\kappa^2(x) > 0$ or $\kappa^2(x) < 0$ across the inhomogeneous region; these modes are classified as body or surface, respectively. We note, however, that these modes are different from those in a uniform medium, where κ^2 is constant. In addition, we also find modes where $\kappa^2(x)$ takes both positive and negative values across the sheet; we call these hybrid modes. Fig. 2 shows an example of a fundamental sausage hybrid mode (solid line) along with the x-component of velocity (dashed line). Firstly, κ^2 varies across the whole domain, being positive in some regions and negative in others. Also, the velocity has maxima where $\kappa^2 > 0$, whereas wave motions are smaller where $\kappa^2 < 0$. The eigenfunction is characterised by regions of different signs of κ^2; a hybrid mode exists. For harmonics, the wave motions are more oscillatory across the sheet, in which case oscillations can occur in regions of both positive and negative κ^2. For all modes, we find $\kappa^2 < 0$ for $|x|/a \gg 1$, and solutions are evanescent outside the current sheet.

Fig. 3a shows the dispersion curves obtained for the case of constant density, ρ_o=ρ_e. Kink and sausage modes are shown as dashed and solid lines, respectively. The horizontal dotted line shows the position of the maximum sound speed, c_s^{max} ($\equiv c_s(0)$). Above this line only body and hybrid modes are

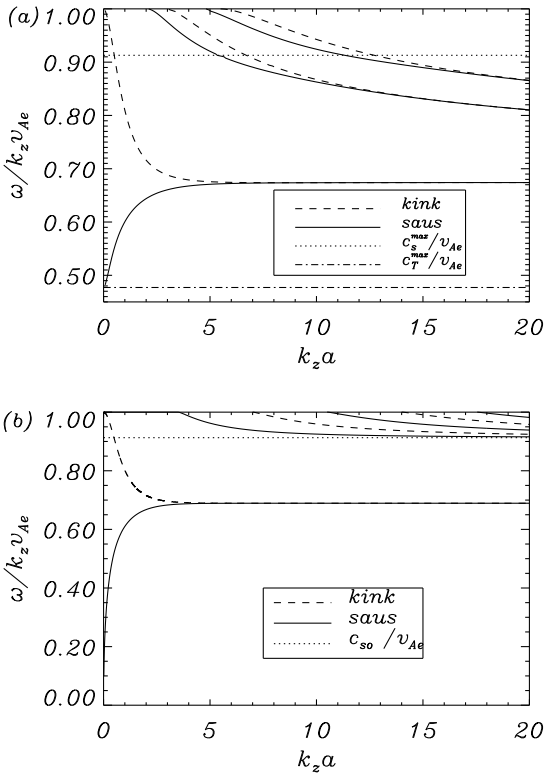

Fig. 3. a The dispersion curves for magnetoacoustic waves in a Harris neutral sheet with uniform density. The modes are classified as *body* when their their phase speed ω/k_z approaches v_{Ae}. A kink and sausage *surface* mode arises. For long wavelength oscillations, the phase speed of the fundamental kink body and sausage surface modes tend to v_{Ae} and c_T^{max}, respectively. For short wavelengths, the phase speeds of both surface modes tend to the same value. Kink and sausage modes above wavenumber cut-offs also exist; these are body or hybrid depending upon the phase speed. The harmonics exist in pairs, their phase speeds merging after the phase speed falls below the maximum sound speed. **b** The dispersion curves for magnetoacoustic waves in the Edwin et al. (1986) slab model for a current sheet (Eqs. 1 and 2), with $R^2 = 2/\gamma$ and $\gamma = 5/3$. Notice, that in the slab model, there is a clear distinction between body and surface modes.

found. For phase speeds close to the maximum Alfvén speed, body modes arise ($\kappa^2 > 0$ for all $|x|/a$ in the structured region). As the phase speed decreases the body modes transform into hybrid modes (κ^2 attains both positive and negative values). The dot-dashed line shows the maximum value of the tube speed c_T^{max}. Below this value only continuum solutions exist (Rae & Roberts 1982 and references therein; see also Seboldt 1990; Poedts & Goossens 1991; Cramer 1994). Between these two lines both surface and hybrid waves arise. Trapped modes exist only in the phase speed range

$$c_T^{max} < \frac{\omega}{k_z} < v_{Ae} \ . \tag{24}$$

The fundamental sausage surface wave (lowest curve in Fig. 3a) is the only mode which exists as a surface wave ($\kappa^2 < 0$ for all $|x|/a$) for all wavenumbers. At long wavelengths ($k_z a \ll 1$) its phase speed falls to the maximum tube speed in the current

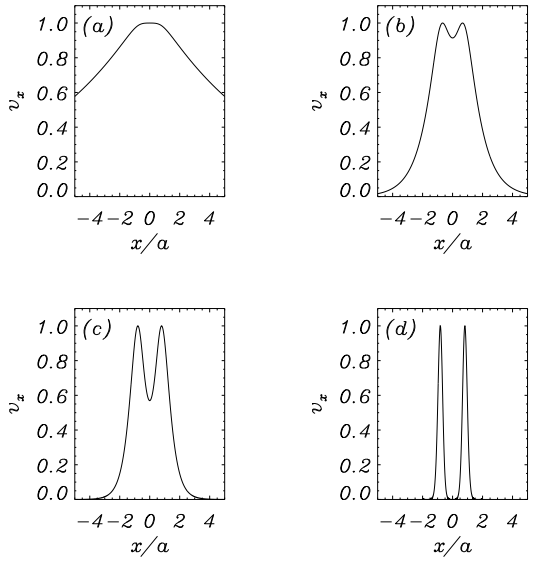

Fig. 4a–d. A plot of the transition from body wave to surface wave for the fundamental kink mode with **a** $k_z a = 0.39$, $\omega = 0.37 v_{Ae}/a$ (body), **b** $k_z a = 1.57$, $\omega = 1.177 v_{Ae}/a$, **c** $k_z a = 3.14$, $\omega = 2.167 v_{Ae}/a$, and **d** $k_z a = 27.5$, $\omega = 18.537 v_{Ae}/a$ (surface modes). Notice that as the mode transforms from being body (oscillatory in sheet) to surface a "dip" appears in the eigenfunction around $x = 0$. As $k_z a$ increases the oscillations become more localised about the edge of the sheet.

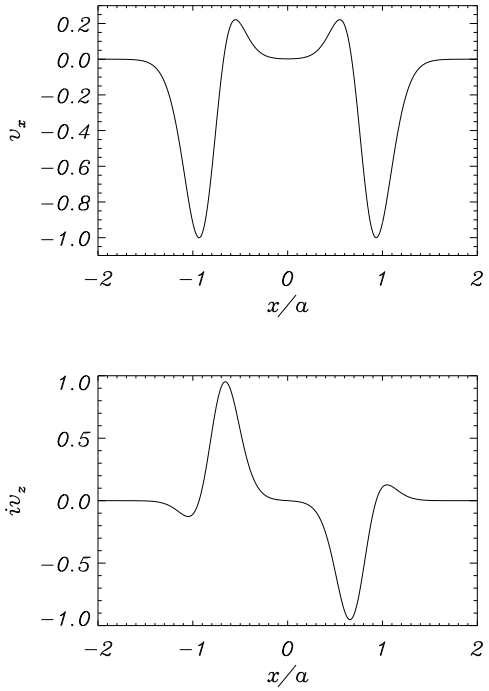

Fig. 5. An example of a first harmonic kink hybrid mode ($k_z a = 27.5$, $\omega = 21.727 v_{Ae}/a$) showing the x (v_x) and z-components (iv_z) of velocity. Two large peaks in the velocity v_x are observed at $x/a \approx \pm 0.9$ (with $\kappa^2 > 0$). In addition, two smaller peaks (of opposite parity to the larger peaks) are seen at $x/a \approx \pm 0.6$ (with $\kappa^2 < 0$). Between $-0.3 < x/a < 0.3$ the velocity is almost zero; wave motions are localised in the exterior of the sheet. The situation for iv_z is similar. Two large peaks (of opposite sign) at $x/a \approx \pm 0.65$ are observed, whereas two smaller peaks are present at $x/a \approx \pm 1.1$. The amplitudes of v_x and v_z are approximately the same.

sheet. As $k_z a$ increases the phase speed increases, tending to a constant value ($\omega/k_z v_{Ae} = 0.675$) for short wavelengths. It is interesting to note that this limiting value at short wavelengths is close to the value given by the slab model of Edwin et al. (1986). If we set $R = \left(2/\gamma\right)^{\frac{1}{2}}$ in Eq. (4), as the ratio of maximum Alfvén speed to maximum sound speed, we obtain a phase velocity of 0.689 for $\gamma = 5/3$, which compares favourably with the numerical results for the Harris sheet.

The fundamental kink wave exists for all wavenumbers, although it is a surface wave only for k_z above a threshold. Fig. 4 illustrates the eigenfunction v_x for the fundamental kink mode. For low $k_z a$ $\left(\omega/k_z \approx v_{Ae}\right)$, the kink wave starts off as a body wave and most of the velocity amplitude is concentrated at the centre of the sheet (see Fig. 4a). As the phase speed decreases the kink mode transforms to a hybrid mode (where κ^2 attains both positive and negative values). As the phase speed falls below the maximum value of the sound speed the mode transforms into a surface wave, where $\kappa^2 < 0$ across the entire sheet (see Fig. 4b, where a small "dip" can be observed in the eigenfunction in the centre of the sheet). For larger $k_z a$, this dip becomes more pronounced (Fig. 4c) so ultimately, for very short wavelengths, there are two peaks in the velocity concentrated near the edge ($x/a \approx \pm 0.9$) of the sheet (Fig. 4d). The phase speeds of the kink and sausage waves approach the same limiting value for short wavelengths.

In a similar way to the work by Edwin & Roberts (1982), magnetoacoustic modes also exist above wavenumber thresholds (Fig. 3a). At the wavenumber threshold $\left(k_z = k_z^{crit}\right)$ the phase velocity equals the exterior Alfvén speed v_{Ae} and the mode is classified as body. As their phase speeds decrease, κ^2 attains both positive and negative values and a hybrid mode forms. The dispersion curve for the fundamental sausage mode, occurring at a critical wavenumber of $k_z^{crit} a = 2.12$, interleaves with the first harmonic kink mode $\left(k_z^{crit} a = 3.06\right)$ when the phase speed falls below the maximum sound speed in the sheet. In addition, the first harmonic sausage mode $\left(k_z^{crit} a = 4.94\right)$ interleaves with the second harmonic kink mode $\left(k_z^{crit} a = 5.50\right)$, and so on. Notice that each merging pair contains a higher overtone kink mode than the sausage. When the "dip" appears in the eigenfunction for the kink mode (Fig. 4) the number of maxima is the same across the sheet for both kink and sausage modes (although the parity about $x/a = 0$ is different). Due to the continuous structuring of sound and Alfvén speed profiles in the current sheet, the phase speeds of these modes do not tend to the maximum value of sound speed, as in the case studied by Edwin et al. (1986). Instead the phase speeds fall below c_s (0); notice how the phase speeds (and therefore frequencies) of these pairs tend to the same value in Fig. 3 after passing through the maximum value of the sound speed. The phase speed tends to an asymptote which is slightly different for each pair of modes. Each pair tends to a slightly higher phase velocity than the previous pair; for the first pair this is 0.69. The value of this asymptote

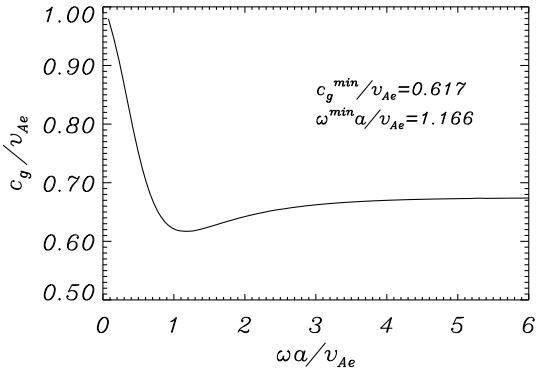

Fig. 6. The dimensionless group velocity c_g/v_{Ae} plotted as a function of dimensionless frequency $\omega a/v_{Ae}$, for the fundamental kink mode. A minimum in the group velocity occurs (c_g^{min}=0.617v_{Ae}) for frequency ω=1.166v_{Ae}/a. Impulsively generated kink waves will therefore show a wavepacket behaviour similar to that described by Roberts, Edwin & Benz (1984). No minima exist for the other modes.

is approximately given by the slab model of short wavelength oscillations in Edwin et al. (1986); see Eq. (4). For short wavelength perturbations we see that the velocity is concentrated about the sheet boundary, whereas for longer wavelengths oscillations across the entire sheet may be expected.

The x and z-components of the velocity are shown in Fig. 5 for a first harmonic kink hybrid wave. This mode is characterised in v_x by two large peaks at $x/a \approx \pm 0.9$, with $\kappa^2 > 0$ ("body") plus two smaller peaks at $x/a \approx \pm 0.6$ with $\kappa^2 < 0$ ("surface") (cf. Fig 4). The z-component of velocity (iv_z) shows similar characteristics to v_x but is of opposite parity about $x/a = 0$. The velocity in the inner part of the sheet $\left(|x|/a < 0.3\right)$ is approximately zero with wave motions concentrated near the edge of the sheet. The amplitudes of the velocity components are similar; this is to be expected since the maximum values of the sound and Alfvén speeds are similar. The eigenfunction of the associated sausage hybrid wave (the mode that transformed from the fundamental sausage body) is very similar, the main difference being the parity of the two solutions about the current sheet centre. The oscillation frequencies approach the same value as $k_z a$ increases (Fig. 3a).

Fig. 6 shows the group velocity curve for the fundamental kink mode. The minimum group velocity is c_g^{min}=0.617 v_{Ae}, occurring at a frequency ω^{min} = 1.166v_{Ae}/a. These values are of importance in the theory of impulsively generated waves (see Roberts, Edwin & Benz 1984, and below). However no minimum in the group velocity exists for the other modes in the uniform density current sheet. The absence of a minimum in the group velocity also arises in the work of Nakariakov & Roberts (1995). Considering coronal loops modelled by different density profiles, they found that the Epstein profile was a special case: it had no minimum, whereas other density profiles possessed minima.

We now examine the driving forces (tension and gradients of gas and magnetic pressure) and the perturbed pressures. This gives some insight into what forces are important in driving

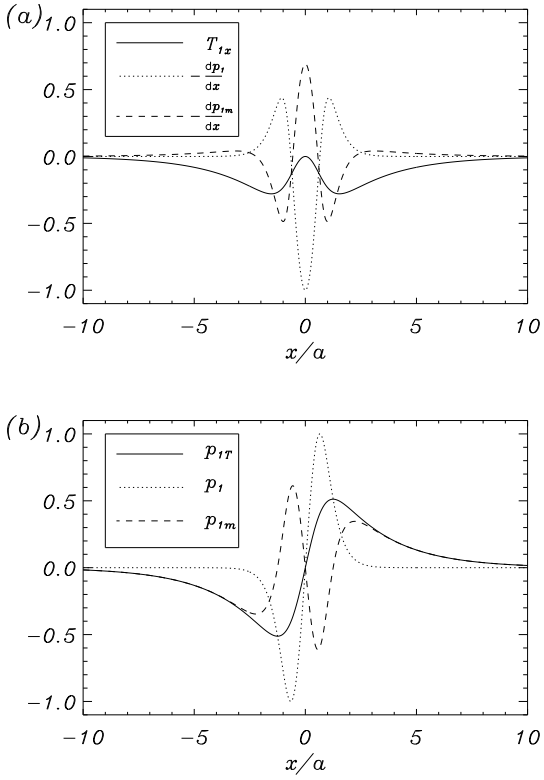

Fig. 7. a The x-component of the driving forces T_{1x}, $-\mathrm{d}p_1/\mathrm{d}x$ and $-\mathrm{d}p_{1m}/\mathrm{d}x$, for the fundamental kink mode with wavenumber k_z = 0.79$/a$ and frequency ω=0.67v_{Ae}/a. The tension forces are very small in the inner part of the sheet $|x|/a$ <1, and the gradients of plasma and magnetic pressure are in anti-phase. In the outer part of the sheet the gradient of the plasma pressure decays rapidly and the magnetic pressure is the greater force. This mode of oscillation therefore possesses characteristics of both fast and slow modes. **b** The perturbed pressures for the same mode. In the central part of the sheet the magnetic pressure (p_{1m}) is out of phase with the plasma (p_1) and the total pressure (p_T) perturbation; this is a feature of the slow mode. In the outer part of the sheet the magnetic and total pressure perturbations are in phase, a feature of the fast mode.

wave motions, and it affords a comparison with the results of a uniform field giving us an indication of whether the modes are fast or slow. The linearised MHD equations (leading to the governing wave equation 13) may be written in the form

$$-\omega^2 v_x = -\frac{i\omega}{\rho}\frac{\mathrm{d}p_1}{\mathrm{d}x} - \frac{i\omega}{\rho}\frac{\mathrm{d}p_{1m}}{\mathrm{d}x} + T_{1x}\ , \tag{25}$$

$$-\omega^2 v_z = -\frac{i\omega}{\rho}\frac{\mathrm{d}p_1}{\mathrm{d}z} - \frac{i\omega}{\rho}\frac{\mathrm{d}p_{1m}}{\mathrm{d}z} + T_{1z}\ , \tag{26}$$

where p_1 and p_{1m} are the gas and magnetic pressure perturbations, p_T (= p_1 + p_{1m}) is the total pressure perturbation, and T_{1x} and T_{1z} are the components of the tension. We first recall the results for a uniform medium, i.e. one in which B, p, ρ (and therefore v_A and c_s) have no x-variation in the region under consideration. From Eqs. (16)-(18) we see that if $\omega/k_z < c_T$ the magnetic pressure is out of phase with both the gas and total pressure perturbation; this is a feature of the *slow* mode. More-

over for this mode, the x-projections of the tension force and velocity are out of phase whereas the z-components are out of phase. For $\omega/k_z > c_T$, the total pressure perturbation, gas pressure and magnetic pressure are all in phase; this is a property of the *fast* mode. In addition, for a fast mode in a uniform medium, T_{1x} is out of phase with v_x whilst the z-components of velocity and tension are in phase.

The formulae for the total pressure p_T perturbation and the tension force $\mathbf{T_1}$ is the same in both uniform and non-uniform media $\left[\mathrm{d}p/\mathrm{d}x + B/\mu\left(\mathrm{d}B/\mathrm{d}x\right) = 0\right]$. However, the perturbed gas and magnetic pressures are altered by the non-uniformity in pressure and magnetic field; see Eqs. (16) and (17). The results show that the magnetoacoustic modes of a current sheet case are more difficult to classify than those of a uniform medium, with the non-uniformity playing an important role.

The results for the non-uniform current sheet are illustrated in Fig. 7 for the fundamental kink mode of frequency ω=0.67 v_{Ae}/a and wavenumber k_z=0.79/a. Fig. 7a shows the driving forces in the x-direction $\left(T_{1x}, -\mathrm{d}p_1/\mathrm{d}x, -\mathrm{d}p_{1m}/\mathrm{d}x\right)$.

Firstly we consider the x-projection of the driving forces (Fig. 7a). In the centre of the current sheet the gradients of plasma and magnetic pressures are clearly out of phase with $|\mathrm{d}p_1/\mathrm{d}x| > |\mathrm{d}p_{1m}/\mathrm{d}x|$; this is a characteristic of a slow mode. Notice also the gradients of gas and magnetic pressures are in anti-phase at $|x|/a \approx 1$, where the amplitudes of the driving forces are approximately the same. In the outer part of the current sheet $\left(|x|/a \geq 1\right)$, the gradient of plasma pressure tends to zero rapidly. In addition, in this region the gradient of magnetic pressure is greater than the gradient of gas pressure; this is a signature of a fast mode. Thus, as we move away from the centre of the sheet, the mode changes from being *slow* in character to being *fast*. This is not surprising since the plasma pressure is maximum (magnetic field minimum) at x/a = 0 whereas the situation reverses as we increase $|x|/a$. In other words we are moving from a high plasma beta regime (where we expect slow waves to dominate) to a low beta region, where fast waves are likely to propagate. Therefore, it is not possible to classify the mode as globally slow or fast; the mode is locally slow in the inner region fast in the outer parts of the structure. Furthermore, unlike the uniform case, due to the non-uniformity in Alfvén speed the x-projection of tension is not out of phase with the velocity. The Alfvén speed is low in the vicinity of the centre of the sheet and therefore tension forces are small. Similar results are also found for the z-component. The gradients of plasma and magnetic pressures are out of phase around the centre of the sheet. As we move away from the centre the gas pressure perturbations become less dominant than magnetic pressure perturbations. In the outer part of the configuration the magnetic pressure becomes greater than the plasma pressure.

These points are reinforced by examining the plasma pressure, magnetic pressure and the total perturbed pressure (Fig. 7b). Notice that the plasma and total pressures are out of phase with the magnetic pressure around $|x|/a \approx 1$. However, as we increase $|x|/a$ the perturbed plasma pressure decays rapidly and the magnetic pressure and the total pressure are in phase for $|x|/a > 2$. Thus for the fundamental modes the oscillations within the sheet are essentially *slow*, whereas the evanescent decaying velocity is predominantly *fast*.

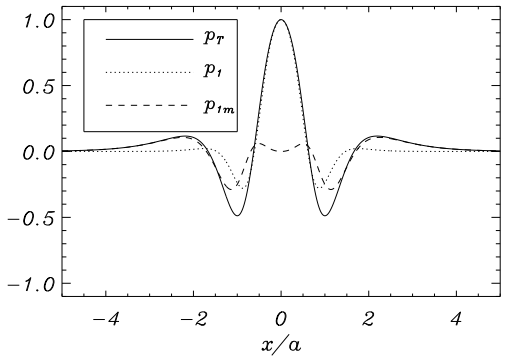

Fig. 8. A plot of the perturbed pressures for the first harmonic sausage hybrid mode, with $k_z a$ = 6.28 and ω=6.12v_{Ae}/a. In the central part of the current sheet $\left(|x|/a < 0.5\right)$ the gas pressure dominates over the magnetic pressure (a slow mode). At $|x|/a$ = 1 the gas and magnetic pressure perturbations are almost in phase with the total pressure perturbation. This is similar to a fast mode. Thus for higher harmonics we may expect *fast* and *slow* modes to simultaneously exist. For $|x|/a > 2$ the mode is fast since the plasma beta is low in this region.

By contrast, for the harmonics of the modes we find that the oscillations within the sheet may possess both fast and slow mode properties. To illustrate this we show the perturbed forces in Fig. 8 for the first overtone sausage hybrid mode with ω = 6.12v_{Ae}/a and $k_z a$ = 6.28. Notice that in the inner part of the current sheet the perturbed magnetic pressure is small (since B is small). Consequently the plasma and total pressure perturbations are almost equal for $|x|/a < 0.5$. This suggests that the mode is slow. However, the perturbations in the outer part of the sheet are different in character. At $|x|/a$ = 1.0 the total, plasma and magnetic pressures are almost in phase. Thus both *slow*- and *fast*-type oscillations occur simultaneously in the sheet for the same velocity component. For $|x|/a > 2$ the pressure term is small and the evanescent decaying velocity has the character of the fast mode. Therefore, in contrast with a uniform medium, there are no pure fast or slow modes in a current sheet. This is due to the non-uniformity in pressure and magnetic field; the plasma beta ranges from infinity at x/a = 0 to zero for $|x|/a \gg 1$. Modes do not possess all the characteristics of slow or fast modes, although we can identify properties of both types in the different regions.

Similar results are found for all modes of oscillation. The tension force in the central part of the sheet is very small, and tension plays an important role only as the Alfvén speed approaches its maximum value. We always see that in the high plasma beta part of the sheet the plasma and magnetic pressures are in anti-phase, with the plasma pressure dominating. In the exterior of the sheet the magnetic pressure is greater than the plasma pressure. For all modes considered we see both slow and fast mode characteristics.

It is interesting to note that in the observations of the neutral sheet oscillations by Bauer et al. (1995a,b) the plasma and

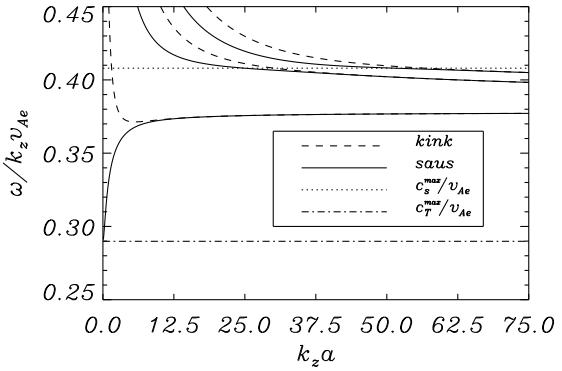

Fig. 9. The dispersion curves for magnetoacoustic wave propagation in a current sheet with an Epstein density profile (8) with an enhancement of ρ_o/ρ_e =5 (c_s^{max} = 0.408v_{Ae}, c_T^{max} = 0.290v_{Ae}). We have only plotted the phase speed over a narrow range. Body and hybrid waves exist in the range $c_s^{max} < \omega/k_z < v_{Ae}$, whilst surface and hybrid waves exist below c_s^{max} and above c_T^{max}. Only continuum solutions exist below c_T^{max}. Modes are classified as either body, surface or hybrid depending upon their phase speed and wavenumber. The modes occur in pairs, the phase speed of each pair merging after they pass through the level c_s^{max}.

magnetic pressures were in anti-phase, in agreement with our theoretical results.

4.2. Epstein density profile

When the plasma density inside the current sheet is no longer equal to the density in the far environment of the sheet, so that $\rho_o \neq \rho_e$, the profile (8) is the Epstein one. The results for an Epstein profile are similar to those in the uniform density case and so we summarise the main results and illustrate the main differences. We take the plasma density at the centre of the current sheet to be five times larger than the constant density away from the current sheet (ρ_o/ρ_e = 5).

The curves in the dispersion diagram are similar to the uniform density case; see Fig. 9. Both kink and sausage, body, surface and hybrid modes may exist. A current sheet therefore supports a rich spectrum of modes. The sausage surface mode, which again exists for all $k_z a$, has a limiting phase speed of the tube speed in the slender current sheet approximation. For short wavelengths the phase speed attains a constant value of $0.38v_{Ae}$. An application of Eq. (4) gives a phase speed of $0.40v_{Ae}$. The fundamental kink mode originates as a body mode $\left(\omega/k_z \approx v_{Ae}\right)$. As the phase speed decreases the body mode transforms into a hybrid mode. When the phase speed passes through the maximum value of the sound speed the mode changes character and becomes a surface wave. The phase velocity of this mode tends to the same value as the sausage surface wave. In addition, body and hybrid waves exist above wavenumber cut-offs: the fundamental sausage mode mode has a threshold of $k_z a$=0.63, first kink harmonic 1.10, first sausage harmonic 1.65 and the second kink $k_z a$=1.96. These cut-offs are lower than in the case of uniform density. These body modes, as in the uniform density case, transform into hybrid waves when their phase speed decreases. Again, a sausage and a kink mode interleave when their phase speed falls below the maximum sound speed within the current sheet. Each kink and sausage mode pair tends to a slightly higher value than the previous pair. We see, however, that for the Epstein density profile, the phase speed only falls below the maximum sound speed level for much higher values of the wavenumber than the case of uniform density. For example, for the fundamental body sausage mode the transition occurs at $k_z a \approx 25$ whilst for uniform density case it is $k_z a \approx 5$.

The driving forces show a similar form to the uniform density case. Due to the large value of $k_z a$ for the phase speed to fall below the maximum sound speed, we find the group velocities possess minima for all modes except the sausage surface. The value of c_g^{min} is approximately the same for all cases considered; namely $0.316v_{Ae}$ for the surface kink mode and approximately $0.356v_{Ae}$ for all the other modes considered. The minimum frequency equals $0.462v_{Ae}/a$ and $2.774v_{Ae}/a$ for the fundamental and first harmonic kink modes, and $1.672v_{Ae}/a$ and 3.846 v_{Ae}/a for the fundamental and first harmonic body sausage modes. Therefore impulsively generated waves will show a similar temporal form to that analysed by Roberts et al. (1984). For coronal loops Nakariakov & Roberts (1995) found minima in the group velocity for a wide variety of density profiles. However, the Epstein profile was an exception where the minimum moved out to infinity.

5. Conclusion and applications

5.1. Summary of results

We have seen that a current sheet may support magnetoacoustic guided waves. The waves are trapped by the inhomogeneity in magnetic field and/or plasma density. Modes may be excited by, say, solar flares, magnetospheric substorms or reconnection. Once excited, the waves may propagate along a current sheet and be the source of reported oscillations in the solar corona and Earth's magnetosphere.

A current sheet supports waves which may be body, surface or hybrid. An examination of the driving forces and perturbed pressures shows that no purely fast or slow modes exist in the structure. Observed oscillations have properties of both types of mode. A sausage surface wave exists for all values of the wavenumber; in the long wavelength limit the phase speed approaches the maximum value of the tube speed in the current sheet. A fundamental kink wave also exists in a current sheet. For long wavelengths (with phase speeds approaching the maximum value of the Alfvén speed in the sheet) the wave is characterised as a body mode ($\kappa^2 > 0$ for all $|x|/a$ in the inhomogeneous region). As the phase speed decreases, κ^2 attains both positive and negative solutions; this is a hybrid mode. For lower phase speeds $\left(\omega/k_z < c_s^{max}\right)$ the mode changes nature and becomes a surface wave ($\kappa^2 < 0$ for all $|x|/a$ in the structured region). For short wavelength oscillations the phase speed of the fundamental kink and sausage surface waves is constant, tending to approximately the value given in the simple slab model of Edwin et al. (1986) [see Eq. (4)]. Harmonics

Table 1. Estimated periods of ducted waves in current sheets

Mode	Corona	Magnetosphere
Surface Sausage	12 sec	2.5 min
Fundamental Kink	3.5 sec	1.45 min
Fundamental Sausage	1.5 sec	19 sec
First Harmonic Kink	1.0 sec	13 sec
First Harmonic Sausage	0.5 sec	8 sec

also exist above wavenumber cut-offs; these may be body or hybrid depending upon the phase speed. The dispersion curves of a pair of kink and sausage modes merge when their phase speeds fall below than the maximum sound speed within the sheet (the fundamental sausage interleaves with the first harmonic kink, first harmonic sausage with second kink and so on). The phase speeds of each pair merge after the phase speed passes through the maximum sound speed. For a uniform density profile, a minimum in the group velocity exists only for the fundamental kink mode, whereas for the Epstein profile minima also exist for other modes. The results are similar to those obtained by Edwin et al. (1986). The main difference is that, due to the continuous structuring, body modes transform into hybrid modes for all harmonics. In the slab model of Edwin et al. body modes were trapped in the phase speed range between the sound speed in the field-free region and the exterior sound speed. In addition, the fundamental sausage mode, which in our case tends to the c_T^{max} for $k_z a \ll 1$, approaches zero as $k_z a \to 0$; in the slab model the tube speed in the field-free region is zero.

5.2. Application to observations

We now apply our results to some observations. For convenience, we use the case of uniform density. For solar applications we consider a constant Alfvén speed in the exterior of the sheet of v_{Ae}=1000 km s^{-1} and a sheet width $2a$ equal to 1000 km. For magnetospheric applications, an Alfvén speed of 500 km s^{-1} is used with a sheet width of $2a$ = R$_{\rm E}$ (=6400 km). The periods determined using our model are given in Table 1. The fundamental surface mode periods are estimated using a value of $k_z a$ = 0.5, whilst the periods for the other modes are estimated at the onset of the modes (i.e. at the cut-off value of $k_z a$). For the coronal case periods lie in the range 0.5 to 12 seconds. Interestingly, periods of this order are frequently reported (see Aschwanden 1987 for a review of radio and X-ray observations). In particular Zlobec et al. (1992) report a 11.4 second oscillation two hours after a solar flare; we suggest this may be due to surface waves in a current sheet. There are many recent reports of short period oscillations, which may be due to magnetoacoustic waves in current sheets. Pasachoff & Landman (1984) and Pasachoff & Ladd (1987) detected intensity variations of the green coronal line with periods between 0.5 and 4 seconds. Short oscillations are also abundantly reported in radio and X-ray emission. For example, Correia & Kauffman (1987) report oscillations of 0.3 seconds in hard X-rays whilst Zhao et al. (1990) give periods of 1.4 and 1.6 seconds in microwaves; Aschwanden (1994) and Karlický & Jiřička (1995) give further examples of short period coronal oscillations.

For the Earth's magnetosphere, our calculations give periods in the range 8 seconds to 2.5 minutes, for the various modes. Therefore the 1-2 minute magnetic field fluctuations of the neutral sheet observed by Bauer et al. (1995a,b) may indeed be due to waves propagating in a neutral sheet. Magnetic variations and boundary motions on time scales from a few minutes to several hours have been explained as "flapping" motions of the tail (Mihalov et al. 1970; Hruška & Hruškova 1970; Hones et al. 1971; Russell 1972). Longer periods may be due to surface waves with $k_z a < 0.5$, or for circumstances with lower Alfvén speeds and/or wider sheets.

It is of interest to consider impulsively generated waves. Suppose that at t = 0 an impulse (such as due to reconnection or an instability) occurs at a location z = 0. This impulse is composed of all frequencies. Then the wave observable at large distances $z = h$ from the initial impulse evolves as follows (Roberts, Edwin & Benz 1984) on the basis of the group velocity curve. The event begins with a periodic phase starting at a time h/v_{Ae} and consisting of low frequency, low amplitude waves; this corresponds to the left-hand branch of the group velocity curve (Fig. 6). The frequency and amplitude of the waves in the periodic phase grow until a time h/c_g^{const}, where c_g^{const} is the constant group velocity at high frequency. This is the onset of the quasi-periodic phase. A train of high frequency waves from the right-hand branch of the group velocity curve are superimposed on the low frequency waves from the left-handside. The amplitude of this phase, in an impulsively excited disturbance, is strongly enhanced due to the superposition of high and low frequency waves (Pekeris 1948; see also Ewing, Jardetzky & Press 1957). The oscillations are quasi-periodic; the amplitude varies inversely proportional to the slope of the group velocity curve. During this phase, the frequency of the high frequency low and high frequency waves continues to decrease, whilst those of the low frequency waves continue to increase. This occurs up to a time h/c_g^{min}, where c_g^{min} is the minimum of the group velocity, when the two frequencies take the same value. This marks the onset of the decay phase. The disturbance then consists of a single frequency ω^{min}, and the plasma continues to oscillate with this frequency although its amplitude decays rapidly.

The durations of the periodic and quasi periodic phases are given by (Roberts et al. 1984)

$$\tau_{dur}^{P} = h\left[\frac{1}{c_g^{const}} - \frac{1}{v_{Ae}}\right] , \tau_{dur}^{QP} = h\left[\frac{1}{c_g^{min}} - \frac{1}{c_g^{const}}\right] . \quad (27)$$

As a numerical example, consider the case of uniform density with the results displayed in Fig. 6. The minimum group velocity is c_g^{min}=0.617 v_{Ae} occurring at a frequency of ω^{min}=1.166 v_{Ae}/a. At high frequency, the group velocity approaches c_g^{const}=0.675v_{Ae}. For solar applications, we assume an observational height h=10^5 km above the impulse and an Alfvén speed of 1000 km s^{-1}; then the periodic phase starts 100 seconds after the impulse and lasts for 48 seconds. The quasi-periodic phase has a duration of 13.9 seconds with a minimum period of 2.7 seconds at the end of the phase. For the magnetosphere consider h =50 R$_{\rm E}$ $\left(3.2 \times 10^5 \text{km}\right)$ and an Alfvén speed of 500 km

s^{-1}. Then the periodic phase begins about 10.5 minutes after the impulse and lasts for 5 minutes. The quasi-periodic phase has a duration of 89 seconds. The decay phase then follows. The periodic phase is relatively low in amplitude and so may not be observable because of noise or poor resolution. In which case, our illustration gives a wavepacket of about 14 seconds duration with a minimum period of 2.7 seconds observable in a coronal current sheet. In the magnetospheric sheet, the observable quasi-periodic phase would last for about 89 seconds, with a minimum period of 34 seconds. Of course, this illustration is for a single pulse initiated at the centre of the sheet. More complicated time signatures may be expected for multiple impulses or pulses that occur away from the centre of the sheet (see the numerical simulations by Murawski & Roberts 1993a,b for the case of a coronal loop). In our equilibrium a pulse will generate the disturbances described plus also a z-component of velocity (v_x and v_z are coupled). Therefore more complicated temporal signatures may result from this coupling.

Acknowledgements. J.M. Smith wishes to thank the United Kingdom Engineering and Physical Sciences Research Council (EPSRC) for financial support and NATO (under Grant CRG 901002) for his visit to Palma, where part of this work was undertaken. R. Oliver acknowledges support from the Spanish Ministry of Science and Education (Grant PB96-0092). J.M. Smith is grateful to J.L. Ballester for kind hospitality during his stay in Palma.

References

Anderson, B.J. 1994, in Solar Wind Sources of Magnetospheric Ultra-Low Frequency waves, eds. Engebretson, M.J., Takahashi, K., Scholer, M., Geophysical Monograph 81, American Geophysical Union, 25
Aschwanden, M.J. 1987, Sol. Phys. 111, 113
Aschwanden, M.J., Benz, A.O., Dennis, B.R., Kundu, M.R. 1994, ApJ (SS) 90, 631
Aurass, H., Kliem, B. 1992, Sol. Phys. 141, 371
Bauer, T.M., Baumjohann, W., Treumann, R.A. 1995a, J. Geophys. Res. 100, A12, 23737
Bauer, T.M., Baumjohann, W., Treumann, R.A., Sckopke, N., Lühr, H. 1995b, J. Geophys. Res. 100, A6, 9605
Birn, J., Hesse, M., Schindler, K. 1996, J. Geophys. Res. 101, 12939
Cally, P.S. 1986, Sol. Phys. 103, 277
Correia, E., Kaufmann, P. 1987, Sol. Phys. 111, 143
Cramer, N.F. 1994, J. Plasma Physics, 51(2), 221
Cramer, N.F. 1995, Physica Scripta T60, 185
Eddy, J.A. 1973, Sol. Phys. 30, 385
Edwin, P.M. 1991, Ann. Geophysicae, 9, 188
Edwin, P.M. 1992, Ann. Geophysicae 10, 631
Edwin, P.M., Roberts, B. 1982, Sol. Phys. 76, 239
Edwin, P.M., Roberts, B., Hughes, W.J. 1986, Geophys. Res. Lett. 13, 373
Epstein, P.S. 1930, Proc. Nat. Acad. Sci 16, 627
Ewing, W.M., Jardetzky, W.S., Press, F. 1957, Elastic Waves in Layered Media, McGraw Hill, New York
Harris, E. 1962, Nuovo Cim. 23, 115
Hones, E.W., Jr., Asbridge, J.R., Borne, S.J. 1971, J.Geophys. Res. 76, 4402
Hopcraft, K.I., Smith, P.R. 1985, Phys. Letts 113A, 75
Hopcraft, K.I., Smith, P.R. 1986, Planet Space Sci. 34, 1253
Hruška, A., Hrušková, J. 1970, J. Geophys. Res. 75, 2449
Karlický, M., Jiřička, K. 1995, Sol. Phys. 160, 121
McKenzie, J.F. 1970, J. Geophys. Res. 75, 5331
Mihalov, J.D., Sonett, C.P., Colburn, D.S. 1970, Cosmic Electrodyn. 1, 178
Montgomery, M.D. 1968, J. Geophys. Res. 73, 871
Murawski, K., Roberts, B. 1993a, Sol. Phys. 119, 399
Murawski, K., Roberts, B. 1993b, Sol. Phys. 145, 65
Nakariakov, V.M., Roberts, B. 1995, Sol. Phys. 159, 399
Pasachoff, J.M., Ladd, E.F. 1987, Sol. Phys. 109, 365
Pasachoff, J.M., Landman, D.A. 1984, Sol. Phys. 90, 325
Patel, V.L. 1968, Phys Letts 26A, 596
Pekeris, C.L. 1948, Theory of Propagation of Explosive Sound in Shallow Water, in Propagation of Sound in the Ocean, Geol. Soc. Am. Memoir 27
Poedts, S., Goossens, M. 1991, Sol. Phys. 133, 281
Priest, E.R. 1982, Solar Magnetohydrodynamics, Reidel, Dordrecht
Rae, I.C., Roberts, B. 1982, MNRAS 201, 1171
Roberts, B. 1981a, Sol. Phys. 69, 27
Roberts, B. 1981b, Sol. Phys. 69, 39
Roberts, B., Edwin, P.M., Benz, A.O. 1984, ApJ 279, 857
Roberts, B. 1985, Magnetohydrodynamic Waves in Solar System Magnetic Fields (ed. Priest, E.R.), Chapter 3, Reidel, Dordrecht
Roberts, B. 1991, Advances in Solar System Magnetohydrodynamics, eds. E.R. Priest & A.W. Hood Cambridge University Press, 105
Roberts, B. 1992, in Sunspots: Theory and Observations, eds. J.H. Thomas & N.O. Weiss, NATO ASI series, Kluwer, 303
Russell, C.T. 1972, Planet Space Sci. 20, 1541
Rušin, V., Minarovjech, M. 1994, IAU Colloq. 144, Solar Coronal Structures, eds. V. Rušin, P. Heinzel, J.-C. Vial, VEDA, Slovakia, 487
Schindler, K., Birn, J. 1978, Physics Reports 47, 2
Schindler, K., Birn, J. 1986, Space Science Reviews 44, 307
Seboldt, W. 1990, J. Geophys. Res. 95, A7, 10471
Singer, H.J., Hughes, W.J., Gelpi, C., Ledley, B.G. 1985, J. Geophys. Res. 90, A10, 9583
Smith, J.M. 1997, PhD Thesis, in preparation
Smith, J.M., Roberts, B., Oliver, R. 1997, A&A 317, 752
Southwood, D.J., Stuart, W.F. 1980, in Dynamics of the Magnetosphere: Proceedings of the A.G.U. Chapman conference on Magnetospheric Substorms and Related Plasma Processes, ed. Akasofu, S.-I, Reidel, Dordrecht, 341
Spitzer, L. 1962, Physics of Fully Ionized Gases, Interscience, Wiley and Sons, New York
Tirry, W., Čadež, V.M., Goossens, M. 1997, preprint
Tsubaki, T. 1988, in R.C. Altrock (ed), Solar and Stellar Coronal Structures and Dynamics, NSO, Sunspot NM, 140
Zhao, R-Y., Jun, S-Z., Fu, Q-J., Li, X-C. 1990, Sol. Phys 130, 151
Zlobec, P., Messerotti, M., Dulk, G.A., Kucera, T. 1992, Sol. Phys 141, 165

This article was processed by the author using Springer-Verlag LaTeX A&A style file *L-AA* version 3.